Soft Matter

Bijel rheology reveals a 2D colloidal glass wrapped in 3D

Journal:	*Soft Matter*
Manuscript ID	SM-ART-03-2022-000407.R1
Article Type:	Paper
Date Submitted by the Author:	09-May-2022
Complete List of Authors:	Ching, Herman; University of California Irvine, Chemical and Biomolecular Engineering Mohraz, Ali; University of California Irvine, Chemical and Biomolecular Engineering

Bijel rheology reveals a 2D colloidal glass wrapped in 3D

Herman Ching and Ali Mohraz*

Department of Chemical and Biomolecular Engineering, University of California, Irvine, CA 92617-2580, USA.

**E-mail: mohraz@uci.edu*

Abstract

We present rheological evidence demonstrating the glass-like nature of bicontinuous interfacially jammed emulsion gels (bijels). Under small amplitude oscillatory shear, bijels exhibited rheological signatures akin to α and β relaxation that are also invariable to interfacial tension changes, behaviors which are reminiscent of caged particle dynamics found in colloidal glasses, and well described by a previously reported adaptation of Mode-Coupling Theory for colloidal glass rheology. Guided by their rheological signatures and supported by particle detachment and attraction energies approximations, we rationalize that bijels can be represented as 2-dimensional (2D) colloidal glasses that percolate in 3-dimensional (3D) space, and attractive interactions are not required for their stability. To provide further support for this conjecture, we qualitatively compare the rheology of bijels and a capillary suspension that is stabilized by strong, rigid capillary bridges between the particles, beyond their limit of linear viscoelasticity. Our results demonstrate that the strong adsorption of particles to the continuous interface and the lack of strong attractive interparticle forces enable recovery by interfacial tension into new jammed configurations after shear deformation. These behaviors are qualitatively different from those in the capillary suspension, where the breaking of attractive interparticle bonds results in dramatic changes to the microstructure and rheology over a narrow range of shear amplitudes. Our findings unveil bijels as 2D colloidal glasses weaving in 3D space and establish that interparticle attractions are not required for stability in bijels, and interfacial jamming alone is sufficient to impart viscoelasticity and gel-like rheology to these materials.

Introduction

Bicontinuous interfacially jammed emulsion gels, or bijels, are multiphase soft materials comprised of interpenetrating co-continuous fluid domains separated by a monolayer of colloidal particles.[1,2] Bijels are typically formed by incorporating a kinetic trap, namely an interfacial jamming step, along the phase separation pathway of a liquid mixture undergoing bicontinuous demixing.[3,4] A commonly used protocol for bijel formation involves preparing a partially miscible binary liquid mixture at its critical composition and rapidly changing its thermodynamic state from miscible to immiscible, for example via a temperature quench as schematically shown in Fig. 1a, in the presence of neutrally wetting colloidal particles.[5] The rapid quench results in spinodal decomposition and the neutrally wetting particles get irreversibly adsorbed onto the fluid-fluid interface.[6] Reduction of interfacial area by phase separation eventually results in colloidal jamming at the interface, which halts demixing and imparts mechanical stability to the mixture.[7,8] The resulting material bears a spinodal-like morphology with co-continuous fluid domains, nearly uniform and tunable domain size,[5,9] and a continuous interface with zero mean, negative Gaussian curvatures.[6,10] Owing to these unique microstructural attributes and their inherent scalability,[3] bijels have attracted considerable attention for functional materials syntheses

such as cell delivery scaffolds and regenerative biomaterials,[9,11] electrochemical device components,[12–18] high surface area catalysts,[19] separation membranes,[20] and structural supports.[21]

While applied research on the use of bijels for materials synthesis has enjoyed significant advances in the past decade, our fundamental understanding of bijels has not experienced similar growth. For example, the rheology of bijels is a rich area with a plethora of interrelated questions at both the microscopic and macroscopic scales that have not yet been fully addressed. In their 2008 article introducing bijels as a new class of soft materials, Clegg and Cates posed the question of whether attractive interparticle interactions are necessary for bijel stability.[6] Here, we rephrase this question as follows: are the rheological properties of bijels best explained in the context of 2-dimensional (2D) colloidal glasses or 3-dimensional (3D) colloidal gels? The 2D glass viewpoint is justified by the jammed particle monolayer that is constrained to the fluid-fluid interface. On the other hand, one can view the particles as having formed a self-supporting network at a low volume fraction (typically $\phi < 0.02$ in bijels) that spans the entire 3D sample volume and imparts mechanical stability to the mixture, an unequivocal signature of colloidal gels.[22] A principal differentiator between these perspectives is the nature of interparticle interactions: dilute colloidal gels require strong (>10 k_BT, where k_B is the Boltzmann constant, and T is the absolute temperature) attractive interparticle interactions to form a percolating network and remain mechanically stable, whereas the interactions in basic colloidal glasses are hard sphere-like, with elasticity arising from particle caging.[23] Since interparticle interactions have a profound impact on the rheology of particulate suspension,[24,25] this relationship can be exploited to investigate the possible importance of attractive interactions for bijel stability. Aside from its scientific significance, the nature of interparticle interactions and its impact on rheology has profound implications for the processability of bijels and the ability to transform them into functional materials.[26] Namely, the bijel processing protocols first pioneered in our laboratory involve a monomer exchange step that can induce Marangoni stresses and cross-flow within the bijel interior, resulting in structural breakdown if the particle monolayer is not strong enough to withstand these effects.[26] Therefore, a deeper understanding of the nature of interparticle interactions in bijels can also pave the way for the chemical library of bijel-derived materials to be expanded, and their technological applications to evolve from proof-of-concept demonstrations to large scale production.

In pursuit of better understanding the underlying physics behind bijel stability, various groups have conducted rheological characterizations of bijels. In 2013, Lee et al. reported a gelation-like event following the formation of water/2,6-lutidine (W/L) and nitromethane/ethylene glycol (NM/PG) bijels, characterized by sharp increases in both the storage (G') and loss (G'') moduli, with a dominating G' signal.[26] The authors also identified notable rheological differences between the two bijels, attributing them to possible system-specific interparticle interactions. In that same year, Imperiali et al. studied a W/L bijel under small amplitude oscillatory shear (SAOS) at various frequencies (ω) and observed a nearly flat $G'(\omega)$ response and a notable minimum in $G''(\omega)$, and cited this behavior as soft glassy-like.[27] Bai et al. later revealed an aging behavior following the formation of non-polar bijels and attributed it to the rearrangement of particles at the interface.[28] Rumble et al. and Tavacoli et al. separately compressed bijels and reported anisotropic rearrangement of the fluid domains, attributing it to particles re-jamming at the interface after deformation.[29,30] Macmillan et al. investigated the yielding of bijels formed by direct mixing and observed a two-step yielding process where the jammed interface appears to be fluidized prior to structural breakdown.[31] These studies concluded that the rheology of bijels is intimately linked to the properties of the particle monolayer, and that particle rearrangements

along the fluid-fluid interface are possible. However, they have not directly addressed the possible necessity of attractive interparticle interactions for stability, and whether they play an important role in bijel rheology.

To address this knowledge gap, here we report a set of experiments that are particularly sensitive to the nature of interparticle interactions, contributing important new information to the existing body of literature on bijel rheology. To enable these tests, we first developed a new bijel system comprising 1,4-butanediol (14BD), propylene carbonate (PC), and neutrally wetting colloidal silica, with physiochemical properties that are suitable for long-duration rheological measurements on a traditional rheometer. These properties include low volatility of the solvents (vapor pressures of 1.1×10^{-2} and 5.8×10^{-2} mmHg at 25°C for 14BD and PC, respectively),[32,33] and an upper critical solution temperature (UCST) of 30.3°C, which renders the miscibility gap easily accessible and enables measurements at near-ambient temperatures.[26] The longevity of this new bijel system allows for rheology tests that are difficult or impossible to perform using most other systems due to possible evaporation of solvents over extensively long testing periods. We performed comprehensive frequency sweep measurements both within and beyond the limit of linear viscoelasticity in bijels. We used temperature as a handle to modulate the interfacial tension, and colloid volume fractions to vary the interfacial curvature, both of which would influence the degree of attractive capillary interactions between the particles,[34] if such forces were significant. These measurements provide critical insights into the dynamics of particle rearrangements in scenarios that are highly sensitive to the nature of interparticle interactions. We demonstrate that the linear rheology of bijels can be fully explained by an early adaptation of the Mode Coupling Theory (MCT) for a soft glassy system, with clear indications that attractive interactions are not responsible for particle localization and viscoelasticity. The frequency response of the bijels within and beyond the limit of viscoelasticity are then compared to a colloidal gel stabilized by capillary bridges as a representative system in which attractive capillary interactions are necessary for stability, highlighting qualitative differences between the two. Overall, our findings indicate that bijels are adequately described as 2D colloidal glasses weaving in 3D space, and attractive interparticle interactions are not responsible for their viscoelasticity and mechanical stability. Our results also shed light on the dynamics of jammed particles along a fluid-fluid interface and the role of particle-laden interfaces in the rheology of the broader class of multiphase mixtures such as Pickering emulsions and solid-stabilized foams. Finally, our findings provide critical insights for designing processing protocols to convert bijels into functional materials, since processability has been shown to be linked to rheology and the nature of interparticle interactions in bijels.[26]

Materials and methods

Materials

The following materials were used as received. 1,3-butanediol (13BD, 99%) was purchased from Acros Organics. 1,4-butanediol (14BD, 99%), propylene carbonate anhydrous (PC, 99.7%), dioctyl phthalate (DOP, 99%), fluorescein isothiocyanate isomer I (FITC, ≥90%), and tetraethyl orthosilicate (≥99.0%) were purchased from Sigma Aldrich. (3-aminopropyl) triethoxysilane (APTES, ≥98%) was purchased from TCI America. Submicron filtered water (HPLC grade) was purchased from Fisher Chemical. Hexamethyldisilazane (HMDS, 98+%) was purchased from Alfa Aesar. Strong ammonia hydroxide solution (27-30%) was purchased from VWR. Anhydrous ethanol (200 proof) was purchased from Rossville Gold Shield.

Development of 14BD/PC bijels

The phase diagram for the 14BD/PC mixture was experimentally determined through a series of cloud point measurements at different compositions, using a custom-made apparatus reported in one of our previous papers.[35] Briefly, weighed amounts of 14BD and PC were added to a 7 mL optical glass cell (Hellma Analytics) with a 10 mm light path, and subsequently heated to 40°C and homogenized by stirring. The cell was then placed into the light path of a custom-made turbidity meter with a temperature probe attachment. A jacketed heat exchanger was used to lower the temperature of the sample at a cooling rate of approximately -0.5°C/min, while concurrently recording the transmitted light intensity and the temperature. We defined the cloud point as the temperature corresponding to a 5% drop in light intensity from the maximum. The 14BD/PC phase boundary was constructed by fitting a 3rd order Fourier series to the cloud point data, and the critical composition and temperature were numerically calculated from the maximum point on the fitted curve. The cloud points and phase boundaries obtained from these measurements are plotted in Fig. 1a. The interfacial tension ($\sigma_{\alpha\beta}$) of the 14BD/PC mixture was measured at different temperatures by using the pendant drop method on a tensiometer (Biolin Scientific Attension Theta) and is plotted as a function of temperature in Fig. 1b.

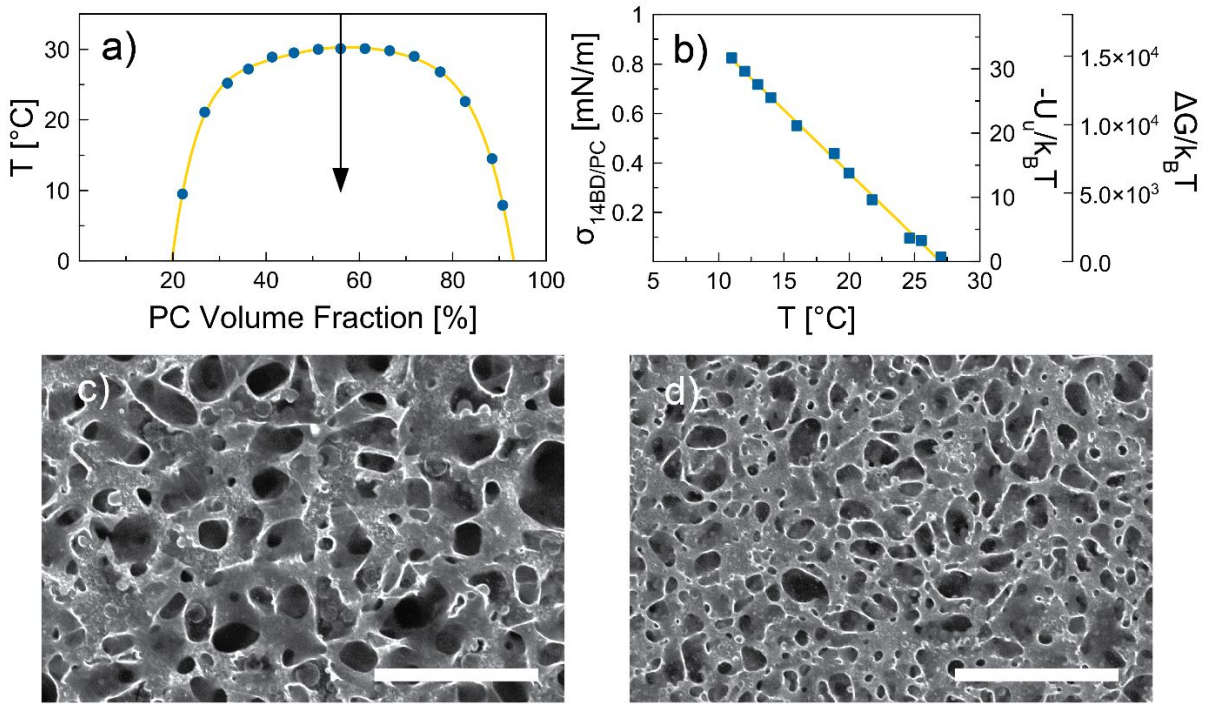

Fig. 1 Physical properties of the 14BD/PC mixture and the formation of 14BD/PC bijels. (a) Phase diagram for the 14BD/PC mixture. The blue circles are measured data, and the yellow line is the phase boundary derived from the Fourier fit. The arrow schematically indicates a quench at the critical composition (56.0 vol% PC). (b) The interfacial tension (left axis) of the 14BD/PC mixture measured (blue squares) at different temperatures. The corresponding detachment energy ($\Delta G/k_BT$) of an adsorbed 310 nm particle and the capillary potential ($-U_w/k_BT$) induced by contact line undulations are plotted on the

right axes. The yellow line is a linear fit drawn to guide the eye. (c,d) CLSM images of 14BD/PC bijels prepared with ϕ_{SNP} = 7.5 × 10^{-3} and 1.5 × 10^{-2}, respectively. Scale bars = 200 μm.

We employed the well-known Stöber process and subsequent silanization of particle surfaces to synthesize monodispersed, fluorescently tagged, and neutrally wetting silica nanoparticles (SNPs) for stabilizing the 14BD/PC bijels.[15,28,29,36] In our experience, the ability to form mechanically stable bijels in the 14BD/PC system strongly depends on the wetting properties of the SNPs, which themselves are sensitive to external factors such as the local temperature and humidity during synthesis. In addition, these wetting properties gradually evolve over time regardless of the storage conditions (vacuum or low temperature), making the particles only usable for a few days after synthesis. Therefore, a fresh batch of neutrally wetting SNPs had to be synthesized every 3 days during our studies, and the extent of silanization needed to produce neutrally wetting SNPs varied between these batches. To account for these variations, we set up six separate reactions simultaneously with different amounts of HDMS in each round of SNP synthesis and assessed particle wettability by their ability to form mechanically stable bijels.[29] First, a silane-coupled fluorescent dye solution was prepared by mixing 8.0 mg of FITC, 33.8 μL of APTES, and 6.4 mL of anhydrous ethanol together for 15 min. Then, in six separate 20 mL scintillation vials, a 1 mL aliquot of the dye solution, 8.8 g of anhydrous ethanol, 1.0 mL of water, 680 μL of tetraethyl orthosilicate, and 295 μL of strong ammonia solution were mixed by vortex mixing (Vortex Genie 2, Science Industries) and placed in a 4°C refrigerator. After 3 h, varying amounts of HMDS (150-200 μL, with 10 μL intervals) were added to the different reaction vials followed by vortex mixing for 15 s, and then allowed to react unperturbed in the refrigerator for an additional 18 h. Typically, one of the six reactions would produce neutrally wetting SNPs, while the others were either too hydrophobic or too hydrophilic to sustain mechanically stable bijels.[29] The resulting SNPs were subsequently washed by repeated centrifugation and resuspension in anhydrous ethanol and dried in a 110°C vacuum oven for 1 h. Scanning electron microscopy (SEM, FEI Magellan 400 XHR) was used to characterize the particle size (radius, a = 160 nm) and distribution (coefficient of variance, CV = 6.7%). A representative SEM micrograph is shown in Fig. S1 (ESI†).

The wetting properties of the SNPs were qualitatively assessed by imaging the samples on a confocal microscope after a temperature quench and testing for successful bijel formation. Here, the criteria for success include the formation of bicontinuous fluid domains (as opposed to solid-stabilized discrete droplets), as well as relative uniformity in the domain size, as assessed by confocal microscopy imaging. To form the bijels, SNPs were first dispersed in a critical mixture of 14BD/PC using an ultrasonic horn (Sonifier 250, Branson Ultrasonics), which provided vigorous agitation and heating. After 30 s of sonication, the final temperature was approximately 50°C, and the dispersion was visually homogenous without any indications of particle aggregation or fluid interface formation. The dispersion was then transferred to a glass cuvette (400 μm ID, VitroCom) preheated to 50°C. Quenching into the 14BD/PC mixture's miscibility gap was achieved by placing the cuvette in direct contact with an aluminum heat sink at room temperature (~22°C). An inverted microscope (rheometer microscopy module, TA Instruments) coupled with a VT-Eye confocal scanner (VisiTech International), or a standalone Olympus Fluoview 3000 confocal laser scanning microscope (CLSM) was used to examine the internal microstructure of the bijels. Fig. 1c and 1d show CLSM (Olympus) images of 14BD/PC bijels formed with ϕ_{SNP} = 7.5 × 10^{-3} and 1.5 × 10^{-2}, where ϕ_{SNP} denotes the volume fraction of SNPs.

Bijel rheology

The rheological measurements presented in this paper were conducted using a stress-controlled rheometer (ARG2, TA Instruments) equipped with a sandblasted, 40 mm diameter, 2° cone-and-plate geometry and a temperature-controlled bottom plate. To maintain consistency, an aliquot of the dispersion from every rheological experiment was also tested for successful bijel formation using CLSM imaging. Bijels were formed directly on the rheometer stage by transferring the homogenized dispersion to a preheated rheometer stage (36°C) and quenching it using the maximum cooling rate available (approx. -16°C/min). A 2 h long SAOS (at strain $\gamma = 1.0 \times 10^{-1}$ % and frequency $\omega = 6.3 \times 10^{-1}$ rad/s) test was applied to monitor the formation behavior during and after quenching. Oscillatory amplitude sweep experiments were conducted by performing three oscillation cycles at a fixed frequency of $\omega = 6.3 \times 10^{-1}$ rad/s and strains spanning from $\gamma = 1.0 \times 10^{-2}$ % to 1.0×10^{3} %. Since amplitude sweeps extend to large strains that plastically deform the microstructure of bijels,[31] each of these tests was conducted on a separate bijel. For small and medium amplitude oscillatory frequency sweeps, six separate tests were conducted in succession on one single bijel, at fixed strains of $\gamma = 1.0 \times 10^{-2}$ %, 1.0×10^{-1} %, 1.0%, 2.0%, 5.0%, and 10%, and frequencies ranging from $\omega = 6.3 \times 10^{-3}$ to 6.3×10^{2} rad/s. The frequency sweeps at $\gamma = 1.0 \times 10^{-2}$ % and 1.0×10^{-1} % were conducted from low-to-high and high-to-low frequencies to demonstrate the repeatability of the linear viscoelastic response. For strains greater than $\gamma = 1.0 \times 10^{-1}$ %, we have occasionally observed sudden drops in both *G'* and *G"* during oscillatory measurements, possibly due to microstructural breakdown of the bijel. It is possible that shearing at high rates promoted particle rearrangement or detachment, which, upon repeated cycles, cascaded into catastrophic microstructural failure.[37] Therefore, frequency sweeps at $\gamma > 1.0 \times 10^{-1}$ % were conducted only from low-to-high frequency.

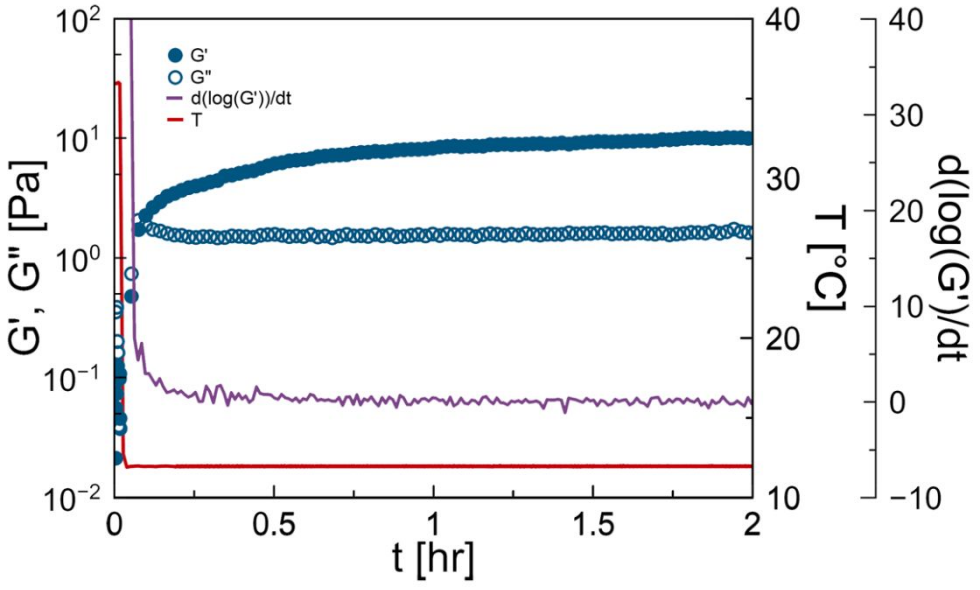

Fig. 2 Time evolution of *G'* (close symbols) and *G"* (open symbols) following the formation of a 14BD/PC bijel with $\phi_{SNP} = 1.5 \times 10^{-2}$. The light blue line (plotted on the right axis) illustrates the temperature quench from 36°C to 12°C. The purple line shows $d\log(G')/dt$, as evaluated numerically from the *G'* values.

Capillary suspension preparation

In our experience, the interfacial tension of the 14BD/PC mixture is too weak to sustain a sample spanning network of dense SNPs at low ϕ_{SNP} against gravitational forces. Therefore, capillary suspensions were formulated using polymethylmethacrylate (PMMA) microparticles grafted with poly-12-hydroxystearic-acid (PHSA) in a mixture of 13BD/DOP, whose interfacial tension, measured via the pendant drop method on a tensiometer is $\sigma_{13BD/DOP}$ = 5.26 mN/m at 12.0°C. Fluorescently tagged PHSA-PMMA particles were synthesized via established protocols.[38,39] In brief, 1.75 g of PHSA, 0.27 g of 2,2'-azobis-isobutyronitrile, 8.00 mg of Nile Red dye, 0.17 g of 1-octanethiol, 32.54 g of methyl methacrylate, and 0.67 g of methacrylic acid were mixed into 21.98 g of hexane and 10.98 g of dodecane, and reacted under full reflux for 2 h at 80°C to produce PMMA particles. Then 0.16 g of N,N-dimethylethanolamine dissolved in 21.98 g of dodecane was added to the reaction flask and reacted for 12 h at 120°C to covalently bond the PHSA to the PMMA particles. The PHSA-PMMA particles were then washed through repeated centrifugation and resuspension in hexane. A sputter coater (EM ACE600, Lecia) was used to deposit a 4 nm layer of iridium onto the particle surface prior to SEM imaging. The resulting iridium-coated PMMA-PHSA particles had an average diameter of 1.05 µm and a CV of 2.1% (shown in Fig. S2, ESI†). Capillary suspensions were prepared via a procedure similar to that outlined by Bossler and Koos.[40] In brief, 22.8 mg of DOP was dispersed in 769.8 mg of 13BD via ultrasonication by an ultrasonic horn for 60 s, which also raised the mixture temperature to approximately 50°C. Once the suspension naturally cooled back down to room temperature, 169.5 mg of dried PMMA-PHSA particles was added to yield ϕ_{PMMA} = 0.20, and subsequently dispersed using an ultrasonic horn. This sonification process was split into three repeated cycles of ~30 s of ultra-sonification and 2 min of resting to avoid overheating. For CLSM characterization, an oil solubilized fluorescent dye (10-5045, ACDelco) was added to the DOP fluid (1 vol% dye) as a tracer to enable imaging of the capillary bridges between the particles.

Capillary suspension rheology

To load the capillary suspension onto the rheometer, the sample was first transferred onto the rheometer bottom plate using a spatula, and then compressed by lowering the prechilled (12.0°C) measuring geometry (sandblasted, 40 mm diameter, 2° cone) to a gap height of 100 µm, which is 40 µm above the required measurement height. Since compression can cause microstructural changes in the suspension, a 500 s^{-1} pre-shear step was applied for 60 s before lowering the gap height to 60 µm. Then, the suspension was pre-sheared again at 100 s^{-1} for 60 s, and subsequently monitored for 10 h via SAOS (γ = 1.0 × 10^{-2} %, ω = 6.3 × 10^{-1} rad/s) while the particle network reformed. Oscillatory amplitude or frequency sweeps were conducted following this formation-and-aging step. Oscillatory amplitude sweep experiments were conducted at a fixed frequency of ω = 6.3 × 10^{-1} rad/s and strains spanning from γ = 1.0 × 10^{-3} % to 1.0 × 10^{3} %. For frequency sweeps, strain amplitudes of γ = 1.0 × 10^{-2} %, 2.5 × 10^{-2} %, 4.0 × 10^{-2} %, and 1.0 × 10^{-1} % were selected based on the results of amplitude sweeps to span the linear viscoelastic region and the transition to non-linearity. Amplitude and frequency sweeps were conducted on separate samples since large strain deformation causes irreversible breakdown of the particle network.

Results and discussion

Characterization of 14BD/PC bijels

Fig. 1a summarizes the phase behavior of the 14BD/PC binary mixture. We recorded an UCST of 30.3°C and a critical composition of 56.0 vol% PC. It is worthwhile to mention that this fluid mixture exhibits a symmetric phase boundary centered near 50% volume fraction, which has been previously hypothesized

as an important attribute for optimal bijel formation.[29] This symmetry allows for direct access from the single-phase into the spinodal region via a temperature quench as well as a near-equal volume split between the two phases.[29] Mechanical arrest of spinodal decomposition was made possible by incorporating neutrally wetting SNPs that were modified using the HMDS silanization method outlined in Materials and Methods. Fig. 1c and 1d display CLSM images of 14BD/PC bijels at two different values of ϕ_{SNP}, demonstrating its effect on the bijel characteristic domain size.

To monitor the formation and assess the mechanical stability of this new bijel system, 2-h long SAOS tests were conducted on samples comprising $\phi_{SNP} = 7.5 \times 10^{-3}$ and 1.5×10^{-2} at 21 and 12°C. An example of these tests is plotted in Fig. 2. In general, the formation of 14BD/PC bijels appears to have the rheological signatures of a gelation process with a sharp increase in both *G'* and *G"* (which happens upon crossing the UCST of 30.3°C), and a prominent *G'*>*G"* signal afterward. Following the formation is a slow aging process where *G'* gradually increases to its terminal value while *G"* plateaus early on, akin to the behavior reported by Lee et al., Imperiali et al., and Bai et al.[26–28] These observations were consistent across all samples that were tested. To quantify the rise in *G*' as seen in Fig. 2, we also numerically evaluate $d\log(G')/dt$ using a forward difference approximation, and plot its 9-point moving average value. Importantly, the results of Fig. 2 indicate that our bijels reach mechanical stability, manifested by a near plateau in both *G'* and *G"*, in approximately 100 min, thus enabling the examination of the role of interparticle interactions in bijel stability after a 2 h waiting period. Separately, we monitored the microstructure of these bijels using CLSM for 2 h and did not observe any coarsening of the fluid domains during this aging period. The gradual rise in *G'* after bijel formation may therefore be related to localized particle rearrangements along the interface that do not amount to appreciable changes in the overall microstructure, a topic that will be discussed in later sections.

The near-steady state shear moduli of the 14BD/PC bijels were recorded at the end of the 2 h aging period and plotted in Fig. S3 (ESI†). Although we have only tested two ϕ_{SNP} and two temperatures, our rheology findings suggest a direct relationship between the shear moduli and ϕ_{SNP} or $\sigma_{14BD/PC}$, where stronger bijels can be formed with either a larger volume fraction of particles or higher interfacial tension, which is consistent with the observation made by Lee et al. on the rheology of W/L bijels.[26] Interestingly, the SAOS moduli of the 14BD/PC bijels are at least an order of magnitude weaker than the reported values for the W/L and polystyrene/polybutene (PS/PB) bijels stabilized with similar solid volume fractions.[26,28] This disparity is likely a result of the differences in interparticle attractions between different bijel systems. For instance, the W/L and PS/PB bijels are known to transition to monogels, a concept first introduced by Sanz et al.,[41] where van der Waals interactions result in a particle network that can remain intact even if the fluids are remixed.[26,28] While the relationship between the shear moduli and van der Waals forces has not been fully explored, the transition to a monogel is a clear indicator for the presence of strong van der Waals attractions between the particles. Therefore, to examine the possible role of van der Waals interactions in our system, we formed a 14BD/PC bijel as described earlier, and after a 2 h waiting period, reheated it to above its UCST to allow remixing of the fluids. Fig. 3 shows confocal microscopy snapshots of this experiment, which confirm that the removal of interfacial tension results in complete re-dispersion of the particle network. Importantly, from this observation, we conclude that van der Waals forces are not responsible for the mechanical stability of 14BD/PC bijels.[26]

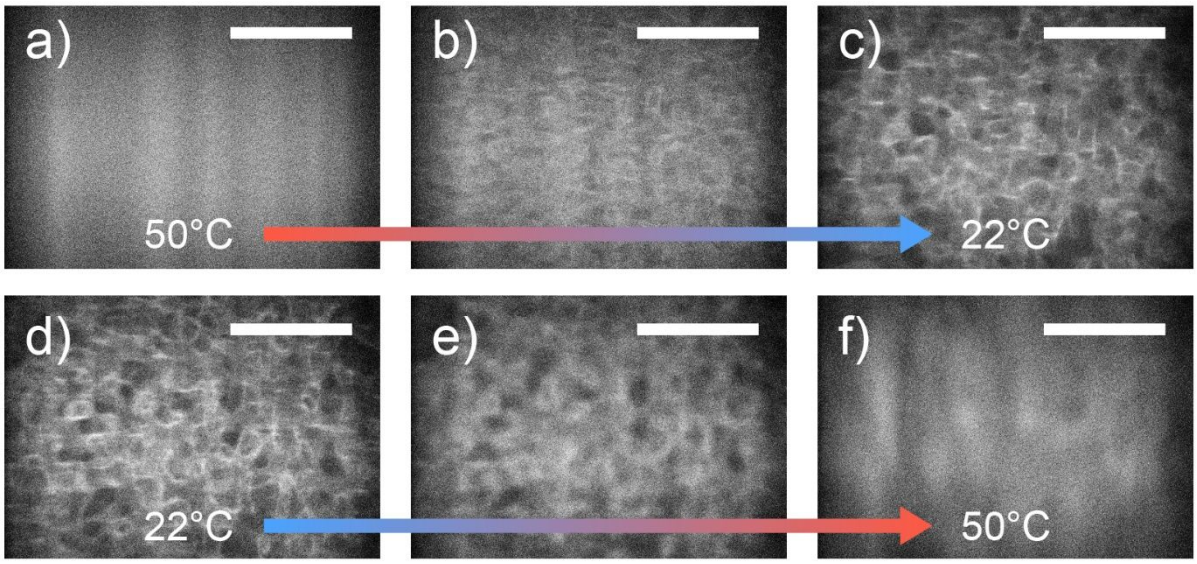

Fig. 3 CLSM (Vt-Eye, VisiTech International) snapshots of the formation and breakdown of a 14BD/PC bijel prepared with ϕ_{SNP} = 1.5 × 10^{-2}. (a-c) A dispersion of SNPs in a critical mixture of 14BD/PC was quenched from 50°C to 22°C. (d-f) After 2 h, the bijel was reheated from 22°C to 50°C. Scale bar = 100 µm.

Having ruled out van der Waals interactions as major contributors to mechanical stability in our system, we now focus on capillary forces between the particles. In bijels, particles may experience attractive capillary interactions through two different mechanisms. First, sequestration of a spherical particle at an interface with negative Gaussian curvature induces quadrupolar deformation to the interface, which in turn promotes attractive capillary interactions between neighboring particles.[42] For a particle with a 90° contact angle, the pair potential for such interactions can be approximated as $U_q = \sigma_{\alpha\beta} c^2 a^4$, where c is the radius of curvature.[34] In this study, ϕ_{SNP} = 7.5 × 10^{-3} and 1.5 × 10^{-2} correspond to average domain sizes of 51.9 and 24.4 µm, respectively, as measured by CLSM imaging. The combination of nm-sized SNPs, weak interfacial tension, and µm-sized domains provide negligible capillary potentials on the order of 10^{-3} k_BT (see Fig. S4, ESI†). Second, and more importantly, topological and chemical heterogeneities on the particle surface can cause undulations in the fluid-particle-fluid contact line, resulting in irregular distortions of the interface in the particle's vicinity, which in turn can cause strong capillary attractions between nearest neighbors.[43] Here, we approximated the deformation due to contact line undulation as quadrupoles and calculated the attraction potential following the formulation derived by Kralchevsky et al.: $U_u = -0.48(\pi\sigma_{\alpha\beta}H^2)$, where H is the undulation amplitude.[44] We asserted an overestimation of H = 10 nm, and computed attraction energy spanning a few to tens of k_BT (see Fig. 1b) for particles in contact. Note that this calculation provides an upper bound for the capillary potential because of the overestimated value of *H*, and the assumption of particles being in contact, which is not the case in the 14BD/PC bijels, given that particles are decorated with a steric layer of trimethylsilyl groups,[45] and that monogels do not form.[28] These approximations suggest that the capillary attractions in 14BD/PC bijels are weak and that long-lasting interparticle bonds are unlikely, which are consistent with the weak shear moduli measured in our experiments. To place the values of U_u in better context, in Fig. 1b we also plot the energy required to detach a particle from the interface,

$\Delta G = \pi a^2 \sigma_{\alpha\beta}(1 - |cos\theta|)^2$, where θ is the three-phase contact angle.[46] A quick comparison between the magnitudes of U_u and ΔG suggests that particle rearrangements along the interface are in principle more freely allowed than movements perpendicular to it, because the energetic cost for in-plane rearrangements, associated with undulating contact lines from particle surface roughness, is much smaller than that of perpendicular motion. This rudimentary assessment suggests that bijels may be well described as 2D colloidal glasses, a conjecture that we will return to in more detail in later sections.

Linear rheology of 14BD/PC bijels

To further investigate the possible role of attractive capillary interactions in our system, we conducted small amplitude frequency sweep experiments at two different colloid volume fractions (modulating the interfacial curvature),[5] and temperatures (modulating the interfacial tension). The results for ϕ_{SNP} = 7.5 × 10^{-3} at the two temperatures studied are plotted in Fig. 4, and are representative of the overall behavior for both colloid volume fractions (see Fig. S5, ESI† for ϕ_{SNP} = 1.5 × 10^{-2}). In all cases, we observe a soft-glassy-like response where *G′* is nearly independent of frequency and *G″* is marked by a prominent minimum near 1.0 × 10^{-1} rad/s.[27] This behavior typically signifies an interplay between distinct fast and slow relaxation mechanisms in an arrested system, and has been observed in colloidal glasses,[47] weak colloidal gels,[48] concentrated emulsions,[49,50] and even polymers and surfactant systems.[51–53] In bijels, the fast and slow relaxation dynamics can be conceptualized as follows. On short time scales, localized thermal motions of a particle rattling against its nearest neighbors rapidly shear the fluids in the particle's vicinity and induce lubrication stresses.[54] Over long periods, such fluctuations can create occasional transitory gaps within the particle network by chance, allowing particles to exchange neighbors or escape cages formed by nearby particles and relax stressed particle cages.[55] Hence, in both high and low frequency regimes, there are noticeable increases in *G″*. This framework also explains the slow aging dynamics that were observed following the formation of 14BD/PC bijels in Fig. 2. Following the initial jamming transition, the minimization of surface area by interfacial tension gradually drives the particle network toward a higher packing state through slow particle rearrangements. These gradual transition toward more tightly packed cages results in a gradual increase in *G′* over time.[56]

In this context, our explanation of bijel rheology as seen in Fig. 4 is reminiscent of colloidal glasses where the frequency scalings of *G′* and *G″* are attributed to the localized Brownian dynamics of caged particles.[57,58] Therefore, to quantify our observations, we propose the use of a rheological model that was derived from Mode-Coupling Theory (MCT) by Mason and Weitz, which incorporates the *α* (slow, out of cage rearrangement) and *β* (fast, in-cage rattling) dynamics of a dense colloidal suspension to describe the frequency scaling of *G′* and *G″* as follows:[57]

$$G'(\omega) = G_p + G_\sigma\left[\Gamma(1-a')cos\left(\frac{\pi a'}{2}\right)(\omega t_\sigma)^{a'} - B\Gamma(1+b')cos\left(\frac{\pi b'}{2}\right)(\omega t_\sigma)^{-b'}\right] + G_D(\omega),$$

$$G''(\omega) = G_\sigma\left[\Gamma(1-a')sin\left(\frac{\pi a'}{2}\right)(\omega t_\sigma)^{a'} + B\Gamma(1+b')sin\left(\frac{\pi b'}{2}\right)(\omega t_\sigma)^{-b'}\right] + G_D(\omega) + \eta_\infty\omega,$$

where G_p is the plateau modulus, t_σ is the *β*-relaxation time, G_σ is the viscoelastic amplitude, G_D is the high frequency modulus, and η_∞ is the high frequency suspension viscosity. a' and b' are critical exponents that are associated with the relaxation time scales and B is the scaling constant in the von Schweidler law.[59] These are predicted by MCT for hard spheres as: a' = 0.301, b' = 0.545, and B = 0.963.

Here, we employed the same parameters as 3D hard sphere glasses since interfacially trapped colloids exhibit in-plane, 2D random walks similar to Brownian motions in 3D,[60] and that previous applications of MCT to 2D systems have revealed similar glass transition features as those in 3D.[61] The equations above were fitted to our data treating the parameters G_p, G_σ, t_σ, G_D, and η_∞ as adjustable, and the results are overlayed in Fig. 4. Overall, this adaptation of MCT captured the essential features of the rheology of bijels, enabling a quantitative assessment of whether the relaxation dynamics of our system are affected by interfacial tension. In Table 1 we report two important parameters extracted from fitting the Mason-Weitz adaptation of MCT to our data: G_p, which describes the magnitude of the *G'* plateau, and the frequency at which *G"* reaches a minimum (ω @ G''_{min}).

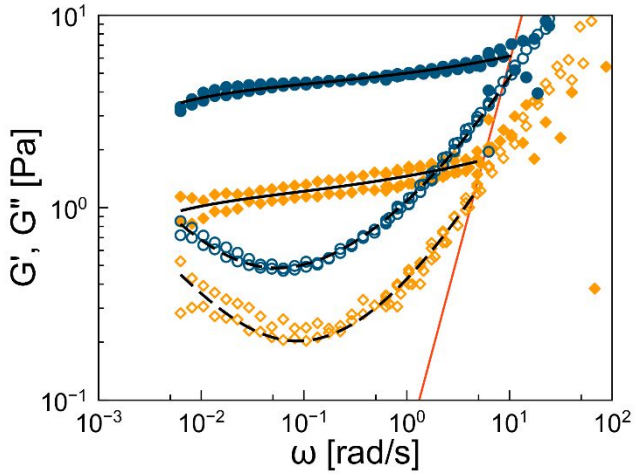

Fig. 4 Frequency response of 14BD/PC bijels comprising ϕ_{SNP} = 7.5 × 10^{-3} at *T* = 12 (blue) and 21°C (orange). *G'* and *G"* are marked by open and close symbols, respectively. The solid and dashed lines represent the MCT fits. The red line indicates the rheometer inertia limit, which is at least an order of magnitude larger than that of the sample itself.[62]

Table 1: Fitted parameters from the MCT model for 14BD/PC bijels at different values of ϕ_{SNP} and *T*. The values for G_p were obtained directly from MCT fits. The frequencies corresponding to the *G"* minimum were numerically calculated from the global minimum of the reconstructed *G"*(ω) using the MCT fitting parameters.

Volume Fraction (ϕ_{SNP}) and Temperature (*T*)	G_p [Pa]	ω @ G''_{min} [rad/s]
ϕ_{SNP} = 7.5 × 10^{-3} *T* = 12°C	4.16	5.53 × 10^{-2}
ϕ_{SNP} = 7.5 × 10^{-3} *T* = 21°C	1.05	8.73 × 10^{-2}
ϕ_{SNP} = 1.5 × 10^{-2} *T* = 12°C	6.31	1.54 × 10^{-1}
ϕ_{SNP} = 1.5 × 10^{-2} *T* = 21°C	2.68	8.83 × 10^{-2}

If attractive interparticle interactions were responsible for the viscoelasticity of bijels, one would expect that an increase in interfacial tension would lead to further arrest of particles and suppression of their slow relaxation dynamics, which would manifest as a shift in the location of G''_{min} to lower frequencies, together with an increase in *G'*. In an earlier study of this concept, Bergenholt et al. expanded MCT to dilute and attractive colloidal gels and demonstrated an ergodicity breaking transition prompted by interparticle attractions in the ranges of a few k_BT.[63] Importantly, their model predicted that the long-time structural decay and the shear moduli exhibit a relaxation time scale that depends on the interaction strength. In other words, a shift in the α relaxation timescale is expected at different attraction potential strengths. Similarly, a shift in the α-relaxation time scale and the location of G''_{min} was observed in colloidal suspensions as particle concentration approaches the glassy limit.[47] Yet, as seen in Fig. 4 and Table 1, *G"* expressed a minimum at approximately the same frequency at both values of *T* (or $\sigma_{\alpha\beta}$) in our bijels, indicating that the α-relaxation timescales are unaffected by interfacial tension. Together with the remixing results shown in Fig. 3, this important observation further corroborates our proposition that attractive interparticle interactions are not responsible for the viscoelasticity of 14BD/PC bijels, and are not required for their mechanical stability. Our explanation for the rises in *G'* and *G"* with $\sigma_{\alpha\beta}$ is that a larger $\sigma_{\alpha\beta}$ would provide greater resistance to shear-induced dilation of the tightly packed interface. More specifically, the viscoelasticity of the interface in bijels stems from the packing of the particles on the interface,[64] whose surface coverage is capped at the jamming limit regardless of the strength of $\sigma_{\alpha\beta}$. At larger $\sigma_{\alpha\beta}$, a larger shear force is needed to stretch the interfaces between the particles, hence the shear moduli are larger. The findings presented in this section suggest that the rheology of bijels in the linear viscoelasticity regime is consistent with that of a jammed particle monolayer without significant attractive interactions, and therefore bijels can generally be viewed as 2D colloidal glasses weaving in 3D space. To provide further evidence for this conjecture, in the next section we compare the rheology of our bijels beyond their limit of linear viscoelasticity to a dilute colloidal gel in which attractive capillary interactions are necessary for stability, and demonstrate qualitative differences between the two.

Beyond linear viscoelasticity: comparison to an attractive system

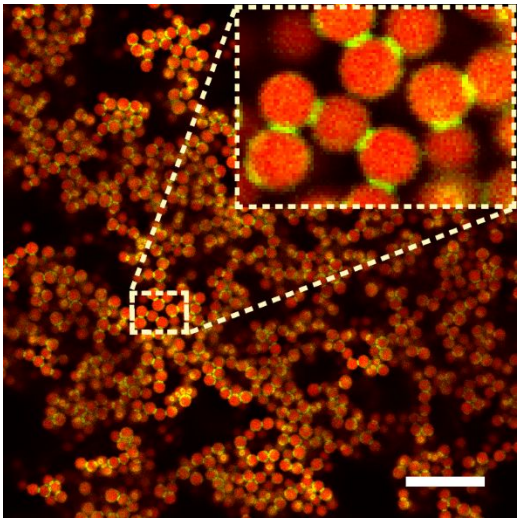

Fig. 5 CLSM image of a capillary suspension prepared with ϕ_{PMMA} = 0.20. The particles are loaded with Nile Red fluorescent dye and shown in red, and the secondary fluid that forms the pendular bridges is

loaded with a green fluorescent dye (see methods) and colorized in green. Inset shows a magnified view (5x) of the suspension. Scale bar = 10 μm.

As a representative example of a dispersion in which capillary interactions are necessary for mechanical stability, we prepared a capillary suspension made of colloidal PMMA particles, 1,3-butanediol (13BD), and dioctyl phthalate (DOP) as the continuous and secondary (bridging) liquid phases, respectively. As demonstrated first by Koos and Willenbacher, including a small amount of a secondary wetting fluid (here DOP) in a suspension can result in particle aggregation due to capillary pendular bridges, and the formation of a sample-spanning particle network.[40,65] Fig. 5 shows a confocal microscopy image of a capillary suspension at ϕ_{PMMA} = 0.20, ϕ_{13BD} = 0.62, and ϕ_{DOP} = 0.08, demonstrating the tenuous particle network held together by pendular capillary bridges of DOP in a continuous 13BD phase. Here ϕ denotes a volume fraction, with the subscript specifying the species. This section will compare the rheology of such a system to our bijels, especially beyond their limit of linear viscoelasticity. We chose this regime because in dilute gels, shear deformation beyond the linear limit typically results in dramatic microstructural, and consequent rheological, changes in a narrow range of strain amplitudes. This behavior is unlike colloidal glasses, where yielding is typically a more gradual event involving changes in the identity of nearest neighbors through cage breaking, without noticeable transformations in the overall microstructure. These distinct features will enable us to further explore signatures of glass-like or gel-like rheological behavior in bijels. To locate the limit of linear viscoelasticity, oscillatory amplitude sweeps were conducted on each system. Fig. 6a-c display the results for bijels at T = 12°C and two different values of ϕ_{SNP} (for a complete set of data on bijels, please see Fig. S6, ESI†), and the capillary suspension at T = 12°C. For bijels, the linear viscoelastic region resides at γ < 0.1%. A gradual transition to non-linearity is observed past this region, where G' slowly drops, eventually resulting in a crossover between G' and G''. Beyond the crossover point, both G' and G'' appear to follow power law scaling with respect to γ, with exponent $n \approx -3/4$. Macmillan, et al. reported irreversible breakdown of the bicontinuous structure of bijels formed by direct mixing at large strains.[31] It is likely that bijels formed through spinodal decomposition experience the same microstructural changes at or near the G'-G'' crossover. For capillary suspensions, the linear viscoelastic regime extends only to $\gamma \approx 0.05\%$, and the transition to non-linearity is marked by a sharp decline in both G' and G'' with a power-law exponent of $n \approx -1$. The local power-law exponents of $G'(\gamma)$, calculated as $n(\gamma) = d(\log(G'))/d(\log(\gamma))$ from the complete set of strain sweep data in Figs. S6 (ESI†) and 6c are plotted in Fig. 6d to quantify the abruptness of the linear to nonlinear transition between the two systems. Although both materials are stabilized by interfacial tension, the role of the interface and its impact on rheology vary dramatically between them. In bijels, shear deformation results in an overall dilation of the particle-laden interface, subsequently reducing the interfacial coverage and loosening the particle network.[66] These events do not result in catastrophic microstructural changes. Instead, the particles remain irreversibly sequestered at the interface, with interfacial tension continuously re-compressing them toward other jammed configurations, provided that the interface remains continuous. As such, the transition to nonlinear viscoelasticity in bijels is a gradual process involving local particle rearrangements along the dilated interface, possible shear-induced reorientation of the fluid domains,[30] and re-jamming of particles into configurations that may slightly differ from the original undeformed state, rendering a small portion of the applied strain unrecoverable. Unlike bijels, however, the limit of linear viscoelasticity in capillary suspensions is determined by the stability of their pendular liquid bridges which form a sample spanning network.[67] At γ > 0.05%, shear deformation can stretch and pinch off the pendular bridges and release the particles from their capillary traps.[68] Since particles are not localized to

a restorative, continuous interface like bijels, such local bond breakages can result in dramatic changes to the microstructure, loss of sample-spanning paths along the particle network, and a precipitous drop in the mixture's viscoelastic moduli. In this qualitative comparison, our results point to clear distinctions between bijels and suspensions with attractive interparticle capillary forces, here in the context of their transition to nonlinear viscoelasticity and yielding.

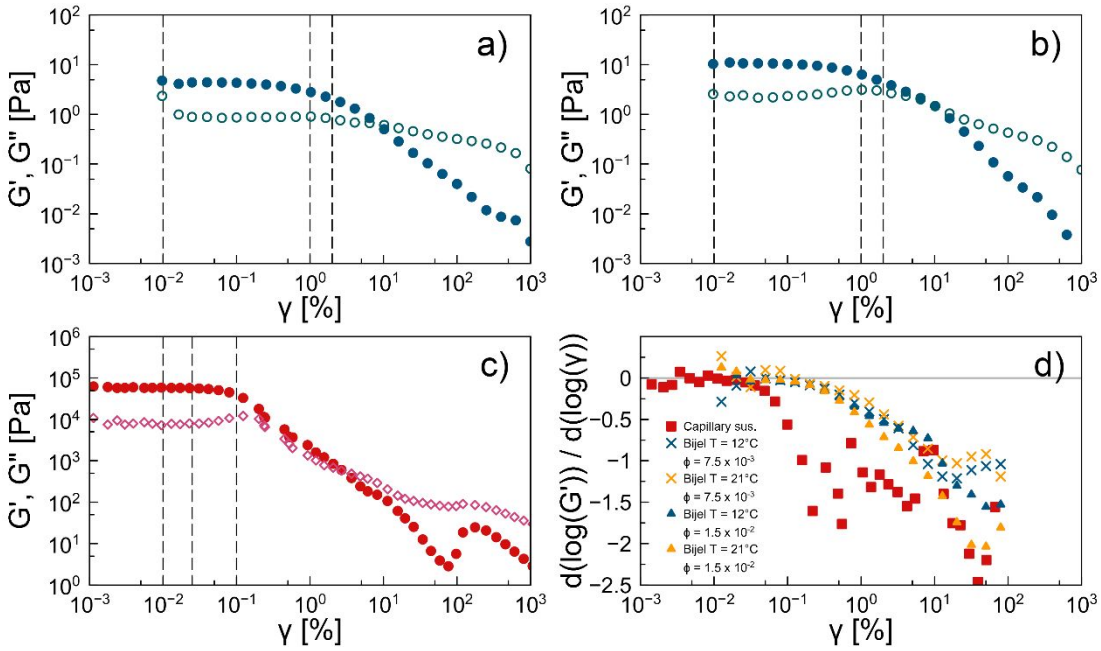

Fig. 6 Oscillatory amplitude sweeps showcasing the transition of G' (close symbols) and G" (open symbols) from linear to non-linear viscoelasticity in 14BD/PC bijels (a-b) and 13BD/DOP capillary suspensions (c). Bijels were prepared with $\phi_{SNP} = 7.5 \times 10^{-3}$ (a) and 1.5×10^{-2} (b), and the capillary suspension was prepared with $\phi_{PMMA} = 0.20$. The dashed lines correspond to the strain amplitudes of the oscillatory frequency sweeps in Fig. 7. (d) Local power-law exponent n(γ) (see text for detail) of G'(γ) for bijels and the capillary suspension.

To further examine the transition to nonlinear viscoelasticity in bijels and capillary suspensions, we performed a series of frequency sweep experiments at different strain amplitudes on each system. The selected strain amplitudes for these tests are marked by dashed lines in Fig. 6, including one baseline test in the linear regime (γ = 0.01% for both systems), one test near the crossover point between *G'* and *G"* (γ = 5% for bijels, γ = 0.1% for the capillary suspension), and an intermediate value to help elucidate the nature of the transition toward yielding (γ = 1% for bijels, γ = 0.025% for the capillary suspension). A subset of the frequency sweep results is shown in Fig. 7 (see Fig. S7-8, ESI† for the complete data set). All bijel results share an intriguing phenomenon where the *G"* valley discussed earlier (recall Fig. 4) gradually disappears as the strain amplitude is increased. The overall values of *G'* also drop as the strain amplitude is increased, but their frequency dependence remains flat. Frequency sweep experiments on bijels examine a rich interplay among several dynamic processes with different timescales, especially at intermediate strain amplitudes where shear deformation can reduce the particle surface coverage. The response is therefore rich and non-trivial. Nevertheless, we believe that the results of Fig. 7 provide important clues that corroborate the representation of bijels as 2D colloidal

glasses weaving in 3D. We explain these results with a focus on the dynamics of particle cage relaxation and re-jamming along the interface. There are likely two phenomena occurring under shear deformation: (1) dilation of the particle-laden interface results in the formation of excess interfacial area and a lower interfacial coverage,[69] effectively dissolving the particles cages to dissipate shear energy, (2) local bending or shearing of the interface forcibly breaks open particle cages,[66] consequently melting the 2D glass network akin to shear-induced melting of a 3D colloidal glass.[70] Unlike colloidal glasses, however, the disruption to the particles cages is simultaneously accompanied by re-compaction by interfacial tension, which increases the surface coverage. At low shear frequencies and large strain amplitudes, the particle network is continually disrupted and loosened by shear, and re-jammed into new mechanically arrested states by interfacial tension. Since cages are persistently being fluidized and rejuvenated, α relaxation is overwritten by shear-induced cage breaking, resulting in a gradual disappearance of the low-frequency rise in *G″* that was discussed in Fig. 4. In other words, because shear deformation dilates the interface, out of cage movement is no longer limited to the exceedingly large timescales associated with α relaxation, and can instead occur on the oscillation timescale. In the high frequency and intermediate strain limit, the interface cannot recoil fast enough for the particles to continuously re-jam by interfacial tension. However, particles remain in proximity and experience local interparticle hydrodynamics interactions caused by ballistic motions of particles barraging against nearby neighbors, giving rise to high frequency responses similar to β dynamics. Therefore, we interpret the gradual disappearance of the *G″* valley at intermediate strains to be associated with shear-induced melting and re-jamming of a 2D colloidal glass that is weaving in 3D. Importantly, our results also indicate that the restorative nature of the continuous interface within bijels provides them with incredible ductility and even self-healing characteristics, a unique attribute that may be exploited for technological applications.

These rheological responses are vastly different in the case of capillary suspensions. In the linear viscoelastic limit, Both *G′* and *G″* appear to follow a mild power law scaling with respect to ω, and no *G″* minimum is observed. Therefore, even in the linear regime, the capillary suspensions do not exhibit the same time-dependent relaxation dynamics as bijels. For these colloidal suspensions stabilized by capillary bridges, the strength of attraction due to the capillary force can be approximated as: $F_c = 2\pi a \sigma_{13BD/DOP} cos\theta \approx 16$ nN.[65] This strong attraction results in a large elastic modulus as seen in Fig. 7g, and also overcomes Brownian forces to lock the particles in their initial arrested configuration. As such, α and β dynamics are suppressed, resulting in a featureless *G″* response. Notably, comparing these results to bijel rheology (Fig. 7a, d, and g) establishes the consequential effects of α and β suppression, which further support our assertion that strong attractions are not present within 14BD/PC bijels, and they are not a requirement for viscoelasticity or stability in bijels. Furthermore, unlike bijels, increasing the strain amplitude (γ = 0.025%, Fig. 7h) did not change the response in the capillary suspension, but a further increase to near the nonlinear regime (γ = 0.1%, Fig. 7i) resulted in dramatic changes where the sweep-up and sweep-down experiments resulted in vastly different responses, likely due to microstructural collapse and breakup of the particle network. This failure mode is consistent with our strain sweep experiments (Fig. 6), which suggested a brittle response in capillary suspensions, due to their short interparticle bonds and the lack of a continuous interface, like that in bijels, to impart them with self-healing characteristics.

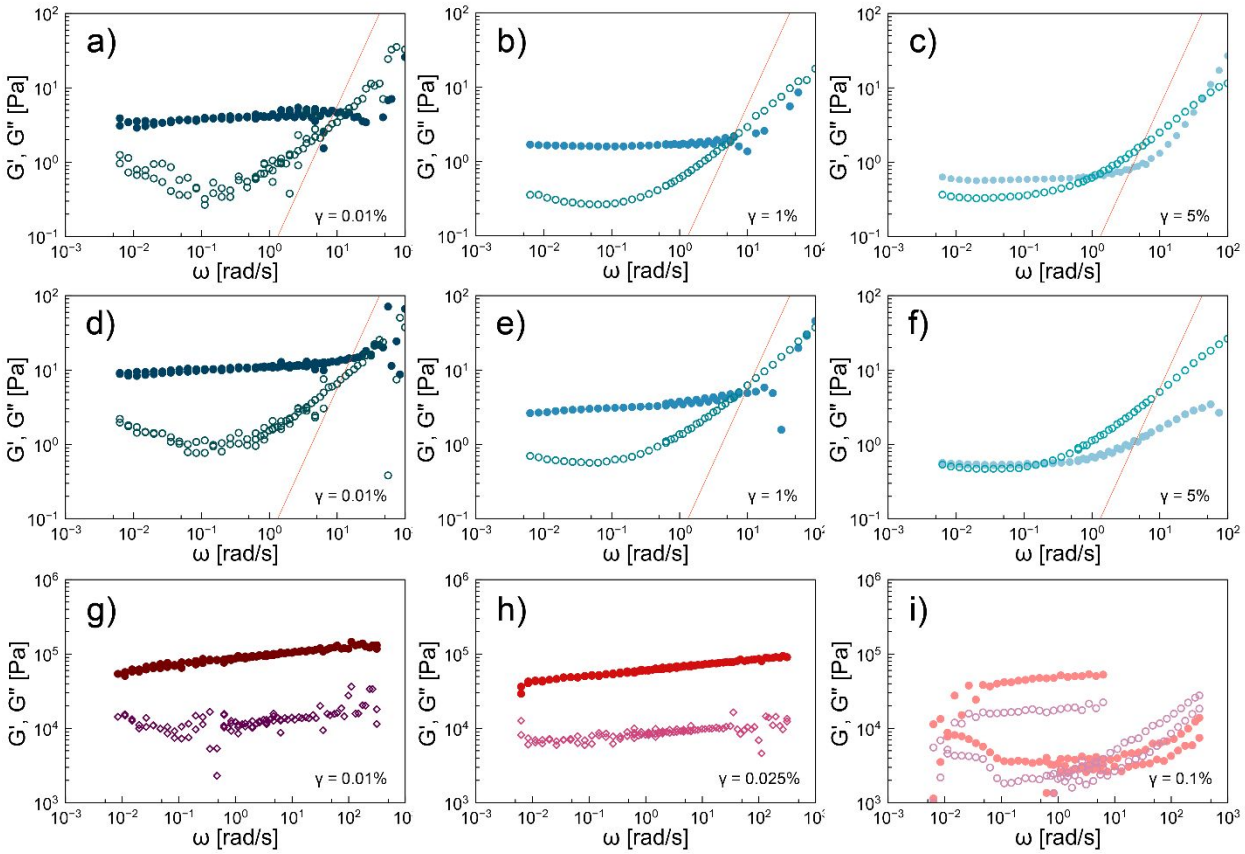

Fig. 7 Frequency response of 14BD/PC bijels (a-f) comprising ϕ_{SNP} = 7.5 × 10^{-3} (a-c) and 1.5 × 10^{-2} (d-f), and 13BD/DOP capillary suspensions (g-i) comprising ϕ_{PMMA} = 0.20 at small and medium strains. *G'* and *G"* are marked by open and close symbols, respectively. The strain amplitude increases from left to right in each row. The red lines indicate the rheometer inertia limit, which is at least an order of magnitude larger than those of the samples themselves.[62]

Conclusion

The nature of interparticle interactions in bijels and the possible necessity of attractive forces for bijel stability were investigated through remixing as well as linear and nonlinear rheological measurements. We ruled out van der Waals forces by performing fluid remixing experiments and used temperature and particle volume fraction as means to modulate the interfacial tension and curvature, in turn tuning the strength of capillary interactions within mechanically stable 14BD/PC bijels. Our linear rheology experiments revealed signatures of long- and short-time relaxation timescales that are invariable to increasing capillary interaction strength, reminiscent of Brownian-driven in-cage (β) and out-of-cage (α) dynamics in colloidal glasses. Nonlinear rheology experiments revealed signatures of cage relaxation and unjammed dynamics at intermediate strains, which we contributed to shear-induced dilation of the continuous interface facilitating in-plane particle rearrangements. Our results also demonstrated remarkable ductility in bijels owing to the strong adsorption of particles to the continuous interface and its regenerative nature, which can continuously re-compress the particles into new jammed configurations. These results were qualitatively compared to a capillary suspension as a

representative system in which attractive interactions are necessary for stability. The capillary suspension showed suppression of α and β dynamics, which we attributed to strong interparticle attractions, along with loss of ductility due to the non-restorative nature of the particle network. Our results indicate that attractive interparticle interactions are not required for stability or responsible for viscoelasticity in bijels, and interfacial jamming alone is sufficient to produce a mechanically stable 2D colloidal glass that percolates in 3D. In addition, our findings provide new insights into the dynamics of particles jammed along fluid interfaces, which have important implications in the design of bijel-derived functional materials and the mechanics of the broader class of solid-stabilized mixtures such as Pickering emulsions.

Conflict of Interest

The authors have no conflicts to declare.

Acknowledgement

This research was funded by the NASA Research Opportunities in Complex Fluids and Macromolecular Biophysics Program (NNX13AQ69G). We thank the UCI Edwards Lifesciences Foundation Cardiovascular Innovation and Research Center for providing access to the Olympus Fluoview 3000 CLSM system (1S10OD025064). The authors acknowledge the use of facilities and instrumentations (SEM and sputter coater) at the UC Irvine Materials Research Institute (IMRI), which is supported in part by the National Science Foundation through the UC Irvine Materials Research Science and Engineering Center (DMR-2011967).

References

1. K. Stratford, R. Adhikari, I. Pagonabarraga, J.-C. Desplat and M. E. Cates, *Science*, 2005, **309**, 2198-2201.
2. P. S. Clegg and J. H. J. Thijssen, in *Bijels: Bicontinuous Particle-stabilized Emulsions*, ed. P. S. Clegg, Royal Society of Chemistry, Cambridge, 2020, ch. 1, pp. 1-33.39.
3. M. F. Haase, K. J. Stebe and D. Lee, *Adv. Mater.*, 2015, **27**, 7065–7071.
4. C. Huang, J. Forth, W. Wang, K. Hong, G. S. Smith, B. A. Helms and T. P. Russell, *Nature Nanotechnology*, 2017, **12**, 1060–1063.
5. E. M. Herzig, K. A. White, A. B. Schofield, W. C. K. Poon and P. S. Clegg, *Nature Materials*, 2007, **6**, 966–971.
6. M. E. Cates and P. S. Clegg, *Soft Matter*, 2008, **4**, 2132–2138.
7. M. Reeves, A. T. Brown, A. B. Schofield, M. E. Cates and J. H. J. Thijssen, *Phys. Rev. E*, 2015, **92**, 032308.
8. J. H. J. Thijssen and J. Vermant, *Journal of Physics: Condensed Matter*, 2018, **30**, 023002.
9. T. J. Thorson, E. L. Botvinick and A. Mohraz, *ACS Biomaterials Science & Engineering*, 2018, **4**, 587–594.
10. M. Reeves, K. Stratford and J. H. J. Thijssen, *Soft Matter*, 2016, **12**, 4082–4092.
11. T. J. Thorson, R. E. Gurlin, E. L. Botvinick and A. Mohraz, *Acta Biomaterialia*, 2019, **94**, 173–182.
12. M. N. Lee and A. Mohraz, *J. Am. Chem. Soc.*, 2011, **133**, 6945–6947.
13. M. N. Lee, M. A. Santiago-Cordoba, C. E. Hamilton, N. K. Subbaiyan, J. G. Duque and K. A. D. Obrey, *J. Phys. Chem. Lett.*, 2014, **5**, 809–812.
14. J. A. Witt, D. R. Mumm and A. Mohraz, *Journal of Materials Chemistry A*, 2016, **4**, 1000–1007.
15. D. Cai, F. H. Richter, J. H. J. Thijssen, P. G. Bruce and P. S. Clegg, *Materials Horizons*, 2018, **5**, 499–505.
16. K. M. McDevitt, D. R. Mumm and A. Mohraz, *ACS Applied Energy Materials*, 2019, **2**, 8107–8117.
17. M. A. Santiago Cordoba, J. S. Spendelow, A. N. G. Parra-Vasquez, L. A. Kuettner, P. M. Welch, C. E. Hamilton, J. A. Oertel, J. G. Duque, E. J. Meierdierks, T. A. Semelsberger, J. C. Gordon and M. N. Lee, *Adv. Funct. Mater.*, 2020, **30**, 1908383.
18. S. J. Gross, K. M. McDevitt, D. R. Mumm and A. Mohraz, *ACS Appl. Mater. Interfaces*, 2021, **13**, 8528–8537.
19. S. Cha, H. G. Lim, M. F. Haase, K. J. Stebe, G. Y. Jung and D. Lee, *Scientific Reports*, 2019, **9**, 6363.
20. M. F. Haase, H. Jeon, N. Hough, J. H. Kim, K. J. Stebe and D. Lee, *Nature Communications*, 2017, **8**, 1234.
21. M.-T. Hsieh, B. Endo, Y. Zhang, J. Bauer and L. Valdevit, *Journal of the Mechanics and Physics of Solids*, 2019, **125**, 401–419.
22. D. Dinsmore and D. A. Weitz, *J. Phys.: Condens. Matter*, 2002, **14**, 7581–7597.
23. E. Zaccarelli and W. C. K. Poon, *Proceedings of the National Academy of Sciences*, 2009, **106**, 15203–15208.
24. K. N. Pham, G. Petekidis, D. Vlassopoulos, S. U. Egelhaaf, P. N. Pusey and W. C. K. Poon, *Europhys. Lett.*, 2006, **75**, 624–630.
25. Z. Shao, A. S. Negi and C. O. Osuji, *Soft Matter*, 2013, **9**, 5492.
26. M. N. Lee, J. H. J. Thijssen, J. A. Witt, P. S. Clegg and A. Mohraz, *Advanced Functional Materials*, 2013, **23**, 417–423.

27. L. Imperiali, C. Clasen, J. Fransaer, C. W. Macosko and J. Vermant, *Materials Horizons*, 2014, **1**, 139-145.
28. L. Bai, J. W. Fruehwirth, X. Cheng and C. W. Macosko, *Soft Matter*, 2015, **11**, 5282–5293.
29. J. W. Tavacoli, J. H. J. Thijssen, A. B. Schofield and P. S. Clegg, *Advanced Functional Materials*, 2011, **21**, 2020–2027.Sdfa
30. K. A. Rumble, J. H. J. Thijssen, A. B. Schofield and P. S. Clegg, *Soft Matter*, 2016, **12**, 4375–4383.
31. K. A. Macmillan, J. R. Royer, A. Morozov, Y. M. Joshi, M. Cloitre and P. S. Clegg, *Langmuir*, 2019, **35**, 10927–10936.
32. T. E. Daubert and R. P. Danner, in *Physical and thermodynamic properties of pure chemicals : data compilation*, Taylor & Francis, Washington, DC, 1989.
33. V. Pokorný, V. Štejfa, M. Fulem, C. Červinka and K. Růžička, *J. Chem. Eng. Data*, 2017, **62**, 4174–4186.
34. M. Oettel and S. Dietrich, *Langmuir*, 2008, **24**, 1425–1441.
35. H. Ching, T. J. Thorson, B. Paul and A. Mohraz, *Mater. Adv.*, 2021, **2**, 5067–5075.
36. N. Hijnen, D. Cai and P. S. Clegg, *Soft Matter*, 2015, **11**, 4351–4355.
37. F. Bonaccorso, S. Succi, M. Lauricella, A. Montessori, A. Tiribocchi and K. H. Luo, *AIP Advances*, 2020, **10**, 095304.
38. M. M. van Schooneveld, V. W. A. de Villeneuve, R. P. A. Dullens, D. G. A. L. Aarts, M. E. Leunissen and W. K. Kegel, *J. Phys. Chem. B*, 2009, **113**, 4560–4564.
39. M. T. Elsesser and A. D. Hollingsworth, *Langmuir*, 2010, **26**, 17989–17996.
40. F. Bossler and E. Koos, *Langmuir*, 2016, **32**, 1489–1501.
41. E. Sanz, K. A. White, P. S. Clegg and M. E. Cates, *Phys. Rev. Lett.*, 2009, **103**, 255502.
42. C. Zeng, F. Brau, B. Davidovitch and A. D. Dinsmore, *Soft Matter*, 2012, **8**, 8582.
43. K. D. Danov, P. A. Kralchevsky, B. N. Naydenov and G. Brenn, *Journal of Colloid and Interface Science*, 2005, **287**, 121–134.
44. P. A. Kralchevsky, N. D. Denkov and K. D. Danov, *Langmuir*, 2001, **17**, 7694–7705.
45. V. M. Gun'ko, M. S. Vedamuthu, G. L. Henderson and J. P. Blitz, *Journal of Colloid and Interface Science*, 2000, **228**, 157–170.
46. R. Aveyard, B. P. Binks and J. H. Clint, *Advances in Colloid and Interface Science*, 2003, **100–102**, 503–546.
47. M. Siebenbürger, M. Fuchs, H. Winter and M. Ballauff, *Journal of Rheology*, 2009, **53**, 707–726.
48. T. Domenech and S. S. Velankar, *Soft Matter*, 2015, **11**, 1500–1516.
49. R. Foudazi, S. Qavi, I. Masalova and A. Ya. Malkin, *Advances in Colloid and Interface Science*, 2015, **220**, 78–91.
50. N. Sanatkaran, M. Zhou and R. Foudazi, *Journal of Rheology*, 2021, **65**, 453–461.
51. S. Ankiewicz, N. Orbey, H. Watanabe, H. Lentzakis and J. Dealy, *Journal of Rheology*, 2016, **60**, 1115–1120.
52. Z. Emami, M. Ehsani, M. Zandi and R. Foudazi, *Carbohydrate Polymers*, 2018, **198**, 509–517.
53. Zs. Németh, L. Halász, J. Pálinkás, A. Bóta and T. Hórányi, *Colloids and Surfaces A: Physicochemical and Engineering Aspects*, 1998, **145**, 107–119.
54. R. A. Lionberger and W. B. Russel, *Journal of Rheology*, 1994, **38**, 1885–1908.
55. H. Zhang, K. Yu, O. J. Cayre and D. Harbottle, *Langmuir*, 2016, **32**, 13472–13481.
56. S. Reynaert, P. Moldenaers and J. Vermant, *Phys. Chem. Chem. Phys.*, 2007, **9**, 6463.
57. T. G. Mason and D. A. Weitz, *Physical Review Letters*, 1995, **75**, 2770–2773.

58. E. Di Cola, A. Moussaïd, M. Sztucki, T. Narayanan and E. Zaccarelli, *The Journal of Chemical Physics*, 2009, **131**, 144903.
59. W. Götze and L. Sjögren, *Phys. Rev. A*, 1991, **43**, 5442–5448.
60. X. Ji, X. Wang, Y. Zhang and D. Zang, *Rep. Prog. Phys.*, 2020, **83**, 126601.
61. F. Weysser and D. Hajnal, *Phys. Rev. E*, 2011, **83**, 041503.
62. R. H. Ewoldt, M. T. Johnston and L. M. Caretta, *Complex Fluids in Biological Systems: Experiment, Theory, and Computation*, Springer New York, New York, NY, 2015.
63. J. Bergenholtz, M. Fuchs and T. Voigtmann, *J. Phys.: Condens. Matter*, 2000, **12**, 6575–6583.
64. Maestro, O. S. Deshmukh, F. Mugele and D. Langevin, *Langmuir*, 2015, **31**, 6289–6297.
65. E. Koos and N. Willenbacher, *Science*, 2011, **331**, 897–900.
66. Maestro and A. Zaccone, *Nanoscale*, 2017, **9**, 18343–18351.
67. F. Bossler, J. Maurath, K. Dyhr, N. Willenbacher and E. Koos, *Journal of Rheology*, 2018, **62**, 183–196.
68. J. Yang and S. S. Velankar, *Journal of Rheology*, 2017, **61**, 217–228.
69. J. S. Bee, D. K. Schwartz, S. Trabelsi, E. Freund, J. L. Stevenson, J. F. Carpenter and T. W. Randolph, *Soft Matter*, 2012, **8**, 10329.
70. C. Eisenmann, C. Kim, J. Mattsson and D. A. Weitz, *Phys. Rev. Lett.*, 2010, **104**, 035502.